Electronic Supplementary Information

High-throughput Computational Screening of Metal Organic Frameworks with Topological Diversity for Hexane Isomer Separations

Liang Peng[a], Qiao Zhu[a], Pinglian Wu[a], Xuanjun Wu[a,*] and Weiquan Cai[b,a,*]

[a]School of Chemistry, Chemical Engineering & Life Sciences, Wuhan University of Technology, Wuhan 430070, P.R. China; [b]School of Chemistry and Chemical Engineering, Guangzhou University, Guangzhou 510006, P.R. China.

Table of Contents

The interactions between framework atoms and hexane isomers were represented by Lennard-Jones (LJ) potential with no consideration of coulomb interaction (equation S1), and cross LJ parameters were estimated by the Lorentz-Berthelot combining rules. All potential parameters are listed in Table S1 and S2 according to UFF [1] and TraPPE [2] force field.

$$U_{ij} = 4\varepsilon_{ij}\left[\left(\frac{\sigma_{ij}}{r_{ij}}\right)^{12} - \left(\frac{\sigma_{ij}}{r_{ij}}\right)^{6}\right] \quad (S1)$$

where i and j are interacting atoms, and r_{ij} is the distance between atoms i and j. ε_{ij} and σ_{ij} are LJ well depth and atomic pair equilibrium distance, respectively.

Table S1. Lennard-Jones parameters of MOFs.[3]

Atom type	ε/k_B [K]	σ[Å]	Atom type	ε/k_B [K]	σ [Å]	Atom type	ε/k_B [K]	σ [Å]
C	47.86	3.47	Zn	62.4	2.46	Co	7.04	2.56
H	7.65	2.85	Zr	34.72	2.78	Cr	7.55	2.69
O	48.16	3.03	Cu	2.516	3.11	Mn	6.54	2.64
N	38.95	3.26	Si	155.99	3.81	B	47.8	3.58

Table S2a. Bond bending potential, Bond stretch potential, Non-bonded Lennard-Jones parameters, Bond torsion potential of hexane isomers

$$U_{bond-bending} = \frac{1}{2}k_\theta\left(\theta - \theta_0\right)^2 \quad (S2)$$

bending	θ_0	k_θ/k_B (K/rad^2)
CH_x-(CH_2)-CH_y	114	62500
CH_x-(CH)-CH_y	112	62500
CH_x-(C)-CH_y	109.47	62500

$$U_{bond-stretch} = \frac{1}{2}k_b\left(r - r_0\right)^2 \quad (S3)$$

stretch	r_0 [Å]	k_b/k_B (K/rad²)
CH_x-CH_x	1.54	96500

Non-bonded Lennard-Jones potentials are calculated by equation S1.

LJ	ε/k_B [K]	σ [Å]
CH_3	108.0	3.76
CH_2	56.0	3.96
CH	17.0	4.67
C	0.8	6.38

$$U_{bond-torsion} = c_0 + c_1\left(1 + \cos\phi\right) + c_2\left(1 - \cos 2\phi\right) + c_3\left(1 + \cos 3\phi\right) \quad (S4)$$

torsion	c_0/k_B [K/rad²]	c_1/k_B [K/rad²]	c_2/k_B [K/rad²]	c_3/k_B [K/rad²]
CH_x-(CH_2)-(CH_2)-CH_y	0	335.03	-68.19	791.32
CH_x-(CH_2)-(CH)-CH_y	-251.06	428.73	-111.85	441.27
CH_x-(CH_2)-(C)-CH_y	0	0	0	461.29
CH_x-(CH)-(CH)-CH_y	-251.06	428.73	-111.85	441.27
CH_x-(CH)-(C)-CH_y	0	0	0	1635.7
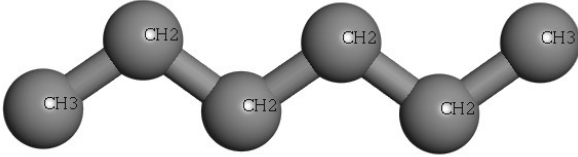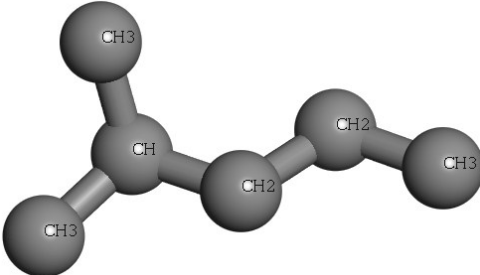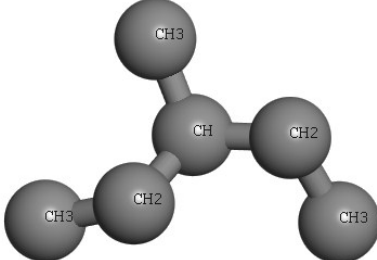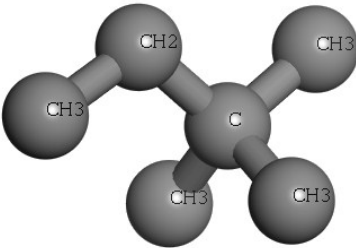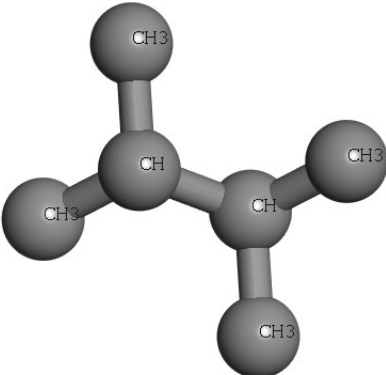
n-hexane (nC6)	2-methylpentane (2MP)
3-methylpentane (3MP)	2,2-dimethylbutane (22DMB)
2,3-dimethylbutane(23DMB)	

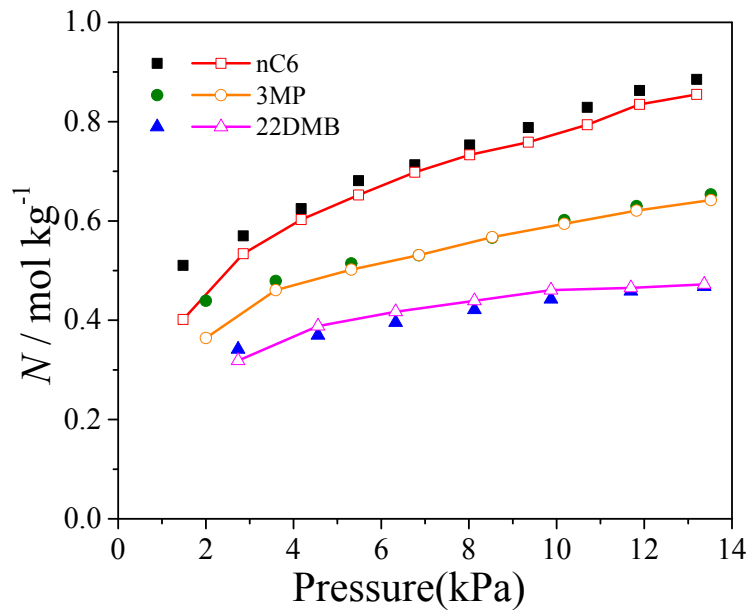**Table S2b.** United-atom models of hexane isomers in TraPPE force field.

Figure S2: Comparison of simulated and experimental adsorption isotherms for nC6, 3MP and 22DMB in Fe-FDCA at 298 K. The solid and hollow points refer to the experimental and simulated data, respectively. The experimental data were taken from reference 4.
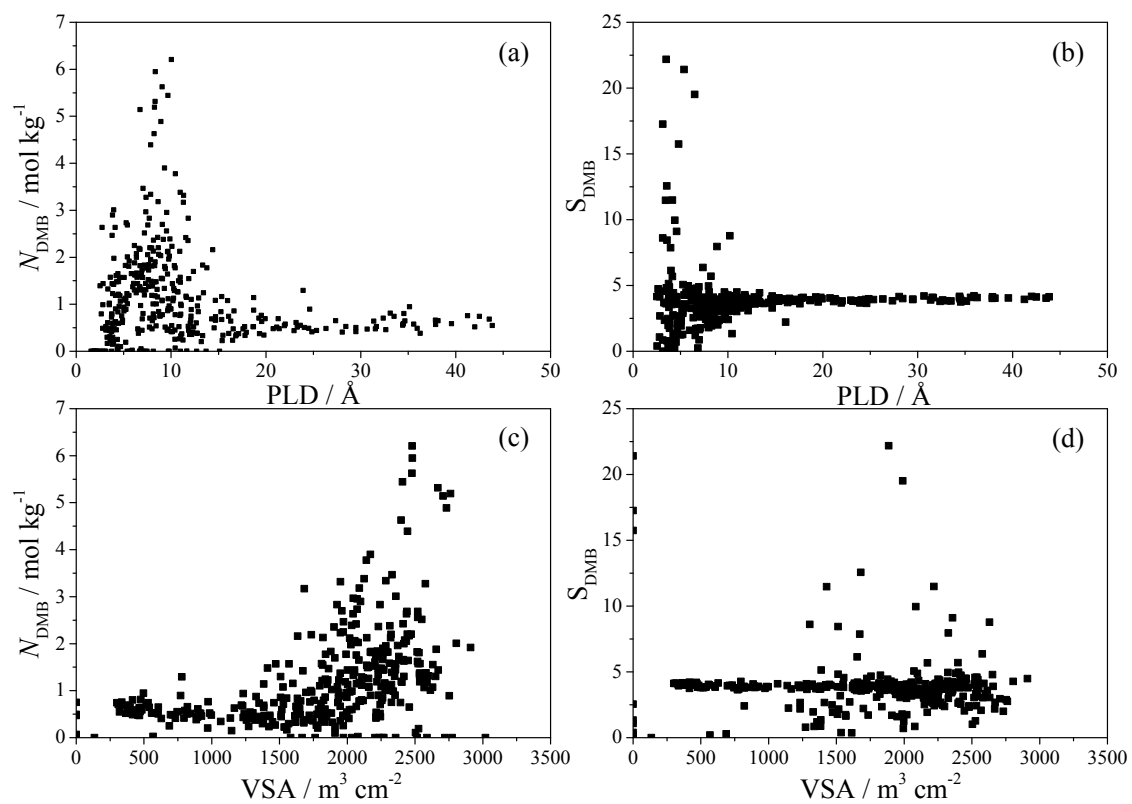
Figure S3. Relationship plots of (a) N_{DMB}; (b) S_{DMB} versus PLD and (c) N_{DMB}; (d)S_{DMB} versus VSA in 390 MOFs at 433 K.
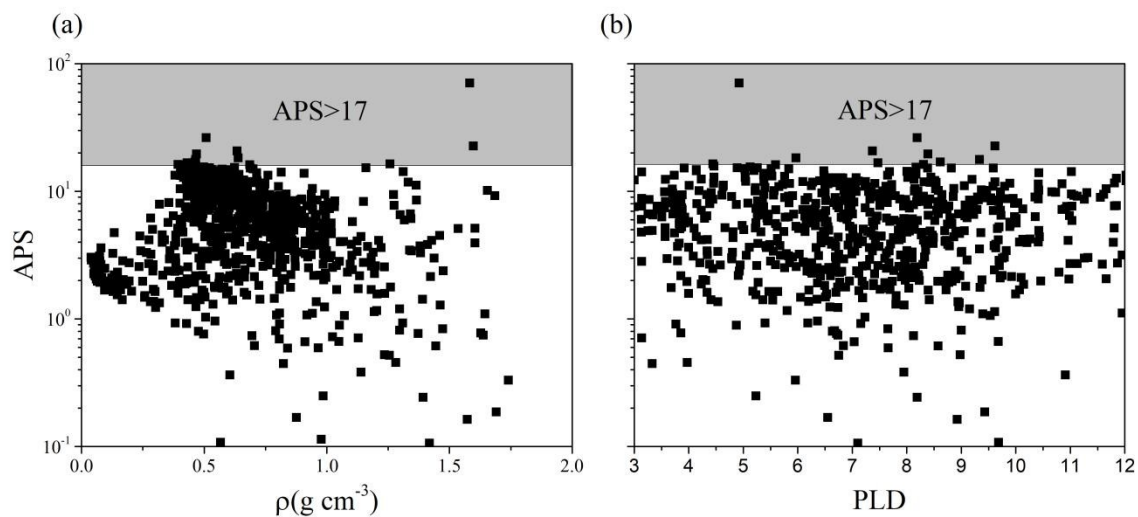
Figure S4. Relationship plots between APS[5] and (a) density; (b) PLD. The shadow region indicates APS > 17.

We explored the relationship plots of APS versus ρ and APS versus PLD for 841 MOFs at 10 bar and 433K. There are 8 MOFs with APS>17 as seen from the shadow region in Figure S4. Neither APS versus ρ nor APS versus PLD shows a good correlation. However, PLD and ρ of the optimal MOFs are in the range of 4.5-10 Å and 0.5-1.7 g cm^{-3}, respectively as shown in Figure S4.
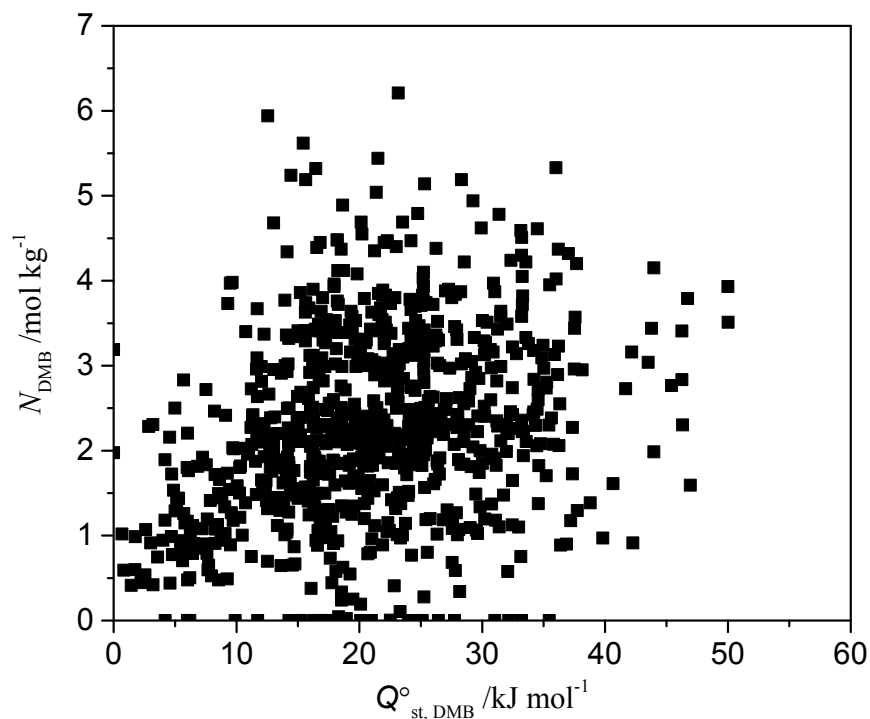
Figure S5. Relationship plots of adsorption capacity versus isosteric heat of adsorption (N_{DMB} ~ $Q^{\circ}_{st,DMB}$) for 22DMB and 23DMB in MOFs.

Figure S5 shows the relationship plots of N_{DMB} versus $Q^{\circ}_{st,DMB}$ for 22DMB and 23DMB in each MOF. N_{DMB} refers to the sum of the adsorption capacities for 22DMB and 23DMB in each MOF, while $Q^{\circ}_{st,DMB}$ is the geometric average of the isosteric heat of adsorption for 22DMB and 23DMB in each MOF. N_{DMB} versus $Q^{\circ}_{st,DMB}$ do not show a good correlation, but the MOFs with the optimal adsorption capacity have $Q^{\circ}_{st,DMB}$ in the range of 15-40 kJ mol^{-1} as shown in Figure S5.

Table S3. Top 22 MOFs with high APS and their physical properties

| No.	MOFs	Topology	Linker	APS	N_{DMB} mol kg^{-1}	S_{DMB}	PLD Å	LCD Å	VSA m^2 cm^{-3}	ρ g cm^{-3}	Q_{st}^{o} kJ mol^{-1}
1	MOF-163	**bct**	L_2	70.59	1.98	35.56	3.97	6.85	2047.25	1.58	43.62
2	MOF-213	**bcu**	L_32	26.28	4.62	5.69	8.21	9.79	2397.44	0.51	29.10
3	MOF-304	**bcu**	L_2	22.69	1.021	22.21	3.49	6.60	2006.56	1.59	35.98
4	MOF-22	**acs**	L_2	20.74	3.27	6.34	7.37	7.98	2577.5	0.63	29.38
5	MOF-3549	**gar**	L_20	19.63	5.19	3.78	6.75	9.89	2458.92	0.46	28.48
6	MOF-4030	**ith**	L_24	18.34	3.79	4.83	5.32	7.85	2361.05	0.63	47.20
7	MOF-3639	**gar**	L_15	17.73	5.33	3.32	7.11	9.93	2369.57	0.46	36.03
8	MOF-4522	**lcsb**	L_5	17.01	4.79	3.55	7.47	10.01	2376.04	0.46	23.89
9	MOF-4521	**lcsb**	L_4	16.73	4.69	3.56	8.11	10.80	2260.71	0.43	20.07
10	MOF-144	**bct**	L_12	16.37	1.64	9.93	4.41	7.50	2086.83	1.25	31.96
11	MOF-3640	**gar**	L_16	16.19	5.04	3.21	9.33	10.79	2409.78	0.39	21.27
12	MOF-4076	**ith**	L_25	16.17	3.41	4.74	5.67	8.41	2326.83	0.68	46.42
13	MOF-3361	**ftw**	L_24	15.52	4.08	3.81	7.93	16.03	2227.82	0.49	18.73
14	MOF-4335	**lcsb**	L_4	15.44	4.55	3.39	8.13	11.45	2249.98	0.43	20.60
15	MOF-4161	**ith**	L_15	15.35	3.51	4.37	5.59	8.01	2220.34	0.62	50.12
16	MOF-4094	**ith**	L_41	15.32	4.47	3.42	8.09	10.61	2322.85	0.43	21.87
17	MOF-8583	**rht**	L_15	15.29	3.72	4.11	7.28	16.02	2219.92	0.52	17.26
18	MOF-2360	**fcu**	L_14	15.29	1.741	8.78	4.83	8.43	2254.99	1.15	28.04
19	MOF-4043	**ith**	L_38	15.25	3.96	3.85	7.24	12.13	2259.83	0.43	17.33
20	MOF-4162	**ith**	L_16	15.25	3.97	3.84	6.36	8.62	2361.39	0.51	31.99
21	MOF-117	**bcs**	L_30	15.23	5.14	2.96	6.73	9.02	2707.87	0.51	25.30
22	MOF-5923	**ocu**	L_12	15.19	3.29	4.61	6.54	14.90	2366.18	0.68	26.32
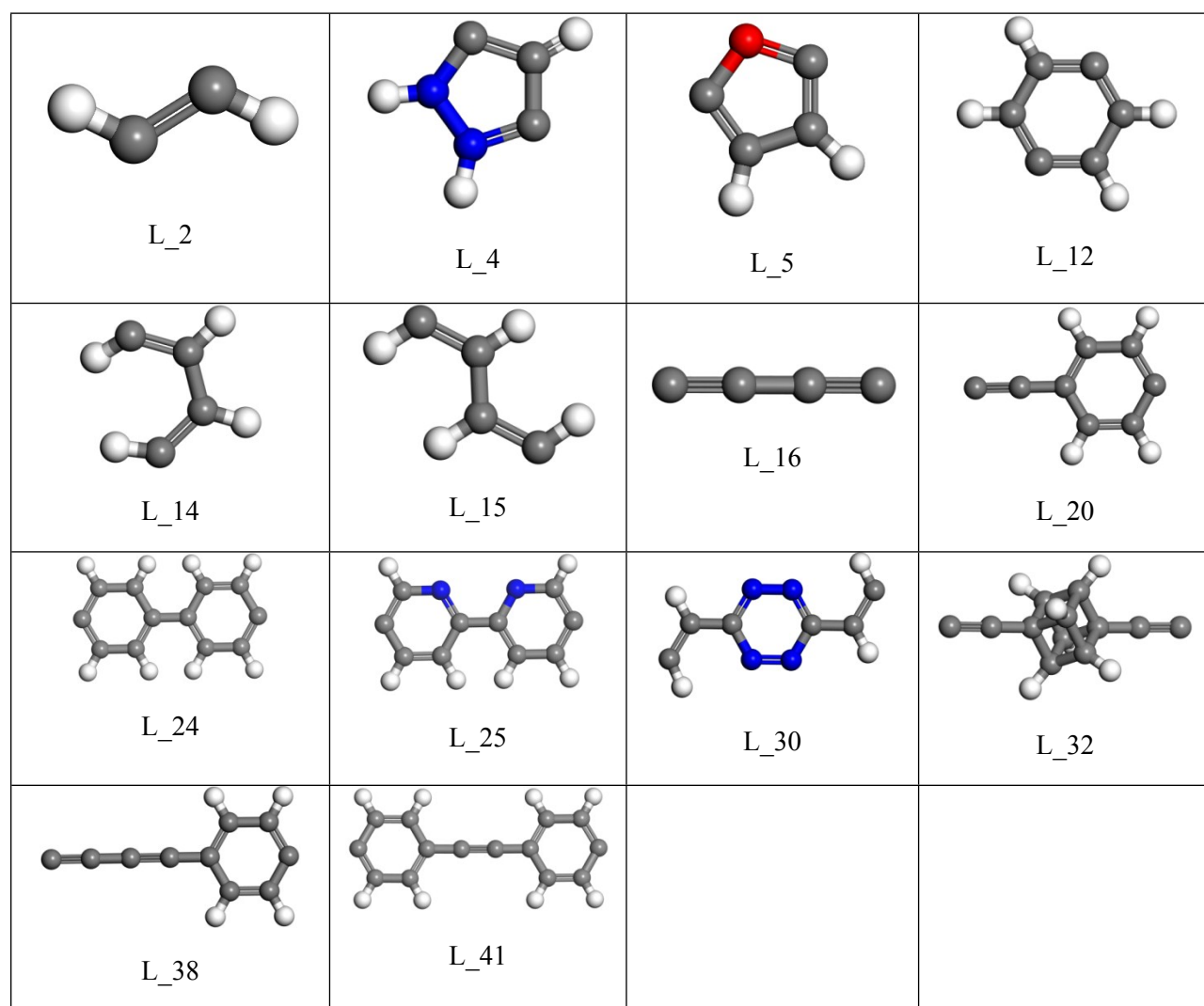
Figure S6. Linkers of top-performance MOFs.[6]

Table S4. Comparison of MOF-163 and real MOFs in terms of adsorption capacities (N) of hexane isomers and selectivities[7-12]

Adsorbents	condition	N (nC6) mol kg^{-1}	N (2MP) mol kg^{-1}	N (3MP) mol kg^{-1}	N (22DMB) mol kg^{-1}	N (23DMB) mol kg^{-1}	S_{DMB}	ref
ZIF-8	423K, 50kPa	0.85	0.25	0.15	0.014	0.038	16.03[a]	7
AC16	303K, 30kPa	1.45	-	0.42	0.09	0.21	6.23[a]	8
XG00-4.5	298K, 10.5kPa	3.01	-	1.15	0.95	-	2.19[a]	9
Zr-bptc	423K, 12kPa	1.43	-	0.248	0.10	-	8.39[a]	10
Zr-abtc	423K, 12kPa	1.204	-	1.02	0.488	-	2.27[a]	10
Zn(BDC)(Dabco)$_{0.5}$	313K, 33.4kPa	0.657	-	0.188	0.116	-	3.61[a]	11
UIO-66_3a	423K, 0.6 kPa	0.034	-	0.119	0.227	0.223	2.94	12
UIO-66_4b	473K, 6.3 kPa	0.093	-	0.19	0.28	0.272	1.95	12
MOF-163_1	433K, 100kPa	0.0059	-	0.0711	1.1384	-	29.57	this work
MOF-163_2	433K, 100kPa	0.0014	0.018	0.043	0.723	0.213	22.5	this work

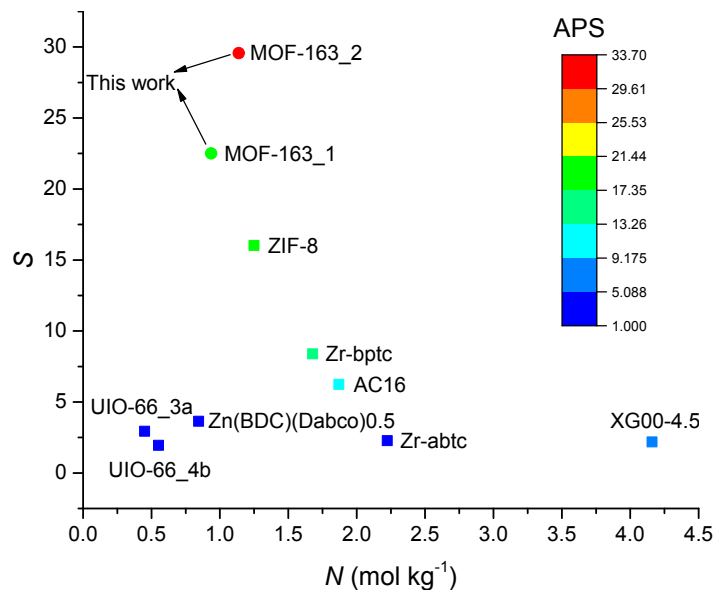[a] The part of experimental data refer to the reverse selectivity of S_{DMB}.

Figure S7. Relationship plots of adsorption selectivity versus total capacity of preferred adsorption components for separation of a multicomponent equimolar mixture (nC6/2MP/3MP /22DMB/23DMB) in various porous materials. The solid circles refer to the simulated data in this work while the solid rectangles refer to the experimental data.[7-12] The experimental data refer to the selectivity for nC6/22DMB except ones of UIO-66 while the data of UIO and MOF-163 refer to the selectivity for 22DMB/nC6. APS of porous materials except UIO and MOF-163 was newly defined as APS=$N_{(nC6+2MP+3MP)}/S_{DMB}$. Total capacity of preferred adsorption components in UIO and MOF-163 refers to $N_{(22DMB +23DMB)}$ while that in the other materials refers to $N_{(nC6+2MP+3MP)}$.
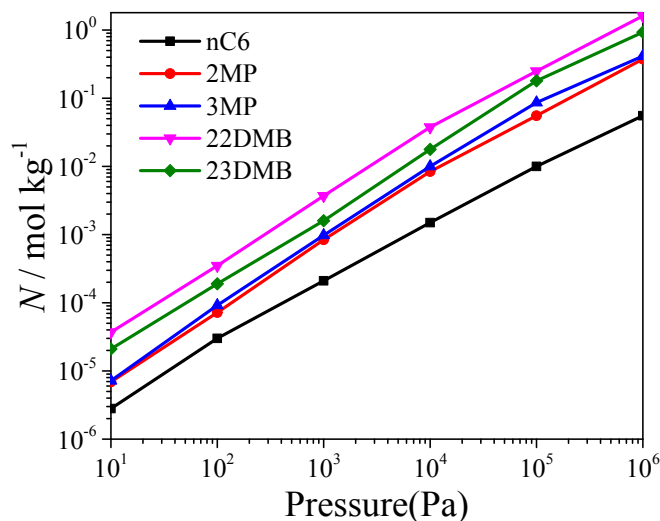

Figure S8. Adsorption isotherms of each component (nC6, 2MP, 3MP, 22DMB and 23DMB) for a quinary equimolar mixture in MOF-9355 (*a.k.a.* **she**-MOF-1) at 433 K.
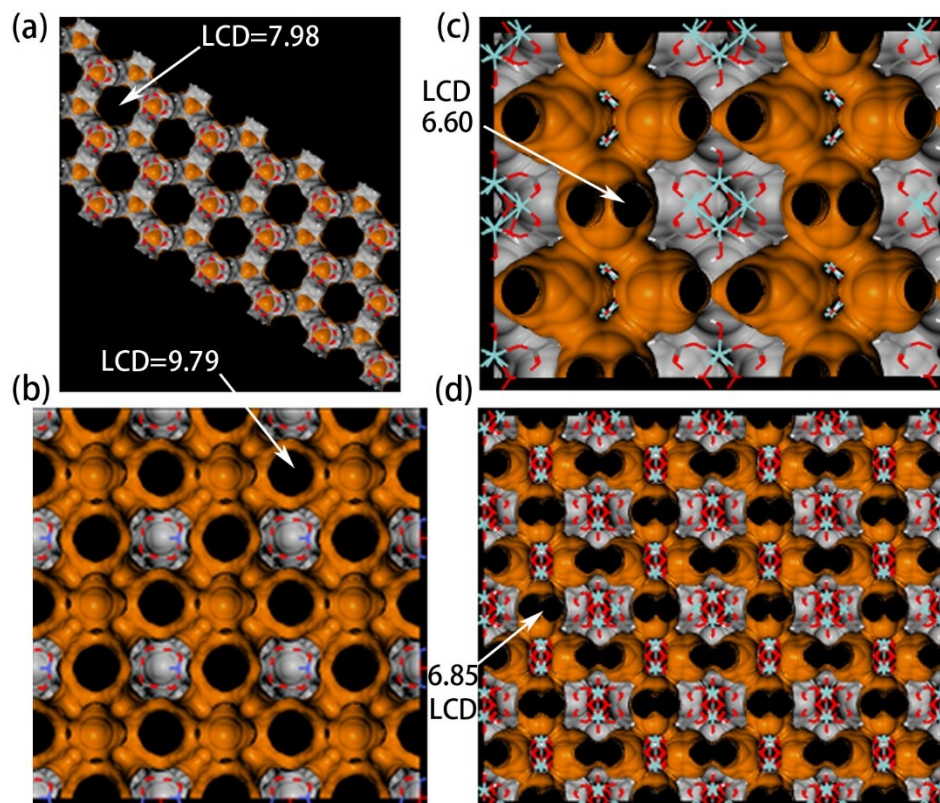
Figure S9. Structures and pore channels of top-performance MOFs.

(a) MOF-22; (b) MOF-213; (c) MOF-304; (d) MOF-163.

Table S5. Parameters used for breakthrough prediction[13]

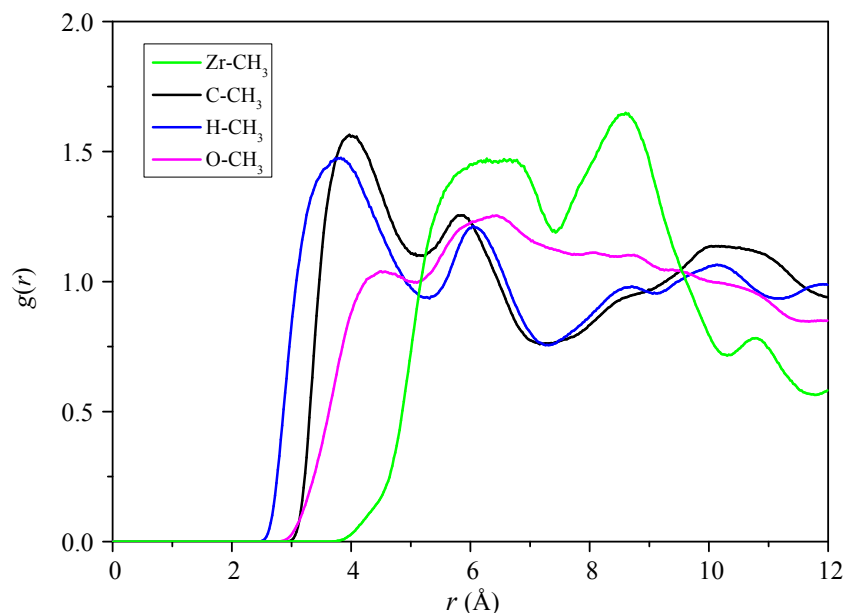| Parameter	Value
Length(L)	0.3m
Inlet Velocity (v_0)	0.04 m/s
Void Fraction (ε)	0.4
Crystal Density (ρ)	1.58 g/cm^3
Bed Pressure (P_0)	1 bar
Column Temperature (T_0)	433 K

Figure S10. Radial distribution functions of various atom pairs between adsorbed 22DMB (CH_3 refers to the methyl group of 22DMB) and the framework atoms (including Zr, C H and O) in MOF-163 at 433 K and 10 bar.

References

(1) Rappé, A. K.; Casewit, C. J.; Colwell, K. S.; Goddard, W. A.; Skiff, W. M. UFF, a Full Periodic Table Force Field for Molecular Mechanics and Molecular Dynamics Simulations. *J. Am. Chem. Soc.* **1992**, *114*, 10024-10035.

(2) Martin, M. G.; Siepmann, J. I. Transferable Potentials for Phase Equilibria. 1. United-Atom Description of N-Alkanes. *J. Phys. Chem. B*. **1998**, *102*, 2569-2577.

(3) Dubbeldam, D.; Krishna, R.; Calero, S. Computer-assisted screening of ordered crystalline nanoporous adsorbents for separation of alkane isomers. *Angew. Che. Int. Edit*. **2012**, *51*, 11867-11871.

(4) Lv, D.; Wang, H.; Chen, Y.; et al. An Iron Based Metal-Organic Framework with Hydrophobic Quadrilateral Channels for Highly Selective Separation of Hexane Isomers. *ACS. Appl. Mater. Inter.* **2018**, 10, 6031–6038.

(5) Altintas, C.; Erucar, I.; Keskin, S. High-Throughput Computational Screening of the Metal Organic Framework Database for CH_4/H_2 Separations. *ACS Appl. Mater. Inter*. **2018**, *10*, 3668-3679.

(6) Gómez-Gualdrón, D. A.; Colón, Y. J.; Zhang, X., et al. Evaluating topologically diverse metal–organic frameworks for cryo-adsorbed hydrogen storage. *Energ. Environ. Sci*. **2016**, *9*, 3279-3289.

(7) Henrique, A.; Rodrigues, A. E.; Silva, J. A. C. Separation of Hexane Isomers in ZIF-8 by Fixed Bed Adsorption. *Ind. Eng. Chem. Res*. **2019**, *58*, 378-394.

(8) Vivo-Vilches, J. F.; Pérez-Cadenas. A. F.; Maldonado-Hódar, F. J., et al. From Carbon Molecular Sieves to VOCs filters: Carbon gels with tailored porosity for hexane isomers adsorption and separation. *Micropor. Mesopor. Mat.* **2018**, *270*, 161-167.

(9) Fernandes, J.; Fernandes, A. C.; Echeverria, J. C., et al. Adsorption of gases and vapours in silica based xerogels. *Colloids Surf. A.* **2019**, *561*, 128-135.

(10) Wang, H.; Dong, X.; Lin, J., et al. Topologically guided tuning of Zr-MOF pore structures for highly selective separation of C6 alkane isomers. *Nat. Commun.* **2018**, *9*(1), 1745.

(11) Bárcia, P. S.; Zapata, F.; Silva, J. A. C., et al. Kinetic Separation of Hexane Isomers by Fixed-Bed Adsorption with a Microporous Metal-Organic Framework. *J. Phys. Chem. B.* **2007**, *111*, 6101-6103.

(12) Patrick, S. Bárcia.; GuimarãEs, D.; Patrícia, A. P. Mendes., et al. Reverse shape selectivity in the adsorption of hexane and xylene isomers in MOF UiO-66. Microporous and Mesoporous Materials, **2011**, 139, 67-73.

(13) Krishna, R.; Long, J. R. Screening Metal-Organic Frameworks by Analysis of Transient Breakthrough of Gas Mixtures in a Fixed Bed Adsorber. *J. Phys. Chem. C.* **2011**, *115*, 12941-12950.